Cement and Concrete Research 42 (2012) 365–376

Contents lists available at SciVerse ScienceDirect

Cement and Concrete Research

journal homepage: http://ees.elsevier.com/CEMCON/default.asp

Prediction of corrosion initiation in reinforced concrete members subjected to environmental stressors: A finite-element framework

Behrouz Shafei [a,*], Azadeh Alipour [a], Masanobu Shinozuka [b]

[a] Department of Civil and Environmental Engineering, University of Massachusetts, Amherst, MA 01003, United States
[b] Department of Civil and Environmental Engineering, University of California, Irvine, CA 92697, United States

ARTICLE INFO

Article history:
Received 10 March 2011
Accepted 2 November 2011

Keywords:
Corrosion (C)
Diffusion (C)
Finite Element Analysis (C)
Chloride (D)
Concrete (E)

ABSTRACT

To study the corrosion of reinforced concrete members subjected to various exposure conditions, a finite-element framework is developed. This framework evaluates the effects of the most critical parameters that may expedite or slow down the corrosion process. Some of these parameters, such as concrete properties and diffusion characteristics, are categorized as internal parameters. In contrast, the environmental parameters, such as ambient temperature, relative humidity, and concentration of carbon dioxide or chloride ions, are considered as external parameters. Using detailed three-dimensional finite-element models, the influential parameters are examined as individual physical environments. The analyses of these environments are based on the concept of transient thermal analysis with appropriate modifications. The novelty of the proposed framework is to consider the nonlinear time-dependent characteristics of the involved parameters along with their mutual interactions. This will result in a more realistic estimation of the extent of degradation over the service life of a structure.

1. Introduction

Corrosion of steel rebars embedded in the concrete is identified as one of the major causes of deterioration in reinforced concrete (RC) members. This phenomenon usually occurs due to the existence of carbon dioxide or chloride ions in the concrete. The penetration of these ions is mostly through the pore structure of the concrete or the concrete micro cracks caused by drying shrinkage or temperature changes [7]. The presence of carbon dioxide or chloride ions in the concrete results in the neutralization of the protective film around the rebar. This increases the vulnerability of steel rebars to corrosive agents. After corrosion initiates, steel is consumed during chemical reaction and it forms a layer of porous material with less strength and more volume compared to original steel. The increasing volume of corrosion products gradually fills out the porous area around the rebar and then pressurizes the surrounding concrete. This causes crack initiation in the concrete and decreases the bond action between the concrete and rebars [7,16,41]. In addition to the concrete degradation, it has been found that the effective cross sectional area and material strength of steel rebars are reduced due to the corrosion process [13–15]. Hence, considering the fact that the corrosion of rebars directly affects both strength and serviceability of RC members [1,2], an accurate estimation of the stage and extent of corrosion is necessary for the reliability analysis and performance assessment of RC members subjected to environmental stressors.

Towards this goal, the current paper proposes a comprehensive finite-element framework to examine the corrosion process in detail and to evaluate its effects on the life-cycle performance of RC structures. This study first identifies the most important parameters that influence the penetration of corrosive agents into the concrete. Some of these parameters, such as concrete properties and diffusion characteristics, are categorized as “internal” parameters, while the environmental parameters, such as ambient temperature, relative humidity, and concentration of carbon dioxide or chloride ions, are considered as “external” parameters. Based on a thorough investigation of available literature and resources, all the required assumptions and coefficients for each of the influential parameters are evaluated and discussed in the finite-element framework. The developed framework utilizes transient thermal analysis and applies the nonlinear time-dependent effects of each parameter to the three-dimensional model of the RC member. By taking advantage of this comprehensive yet rigorous framework, the chloride content at various depths of the RC member is calculated considering the appropriate initial and boundary conditions. The obtained results can be used to determine the chloride initiation time and to evaluate the extent of structural degradation over the service lifetime. This provides engineers and decision-makers with invaluable information to ensure the safety of RC structures while minimizing the associated inspection and maintenance costs.

2. Finite-element framework

To investigate the chloride-induced corrosion in the RC members subjected to various exposure conditions, an integrated finite-element

* Corresponding author. Tel.: +1 413 545 0434.
E-mail address: shafei@engin.umass.edu (B. Shafei).

0008-8846/$ – see front matter © 2011 Elsevier Ltd. All rights reserved.
doi:10.1016/j.cemconres.2011.11.001

framework is developed. This framework evaluates the effects of the most critical internal and external parameters that may expedite or slow down the corrosion process, particularly during the initiation period. Since these parameters are nonlinear in nature and vary over time, they are modeled by following an analogous transient thermal analysis. A transient thermal analysis is capable of calculating the distribution of temperature or similar quantities in the concrete as a function of time. Since the developed framework takes into account the simultaneous contribution of all the influential parameters along with their mutual interactions, it can provide a precise estimation of chloride content at various depths of the concrete.

Through a three-dimensional finite-element model of the concrete, the influential external parameters are examined as individual physical environments. The analyses of these environments are all based on the concept of transient thermal analysis but with appropriate modifications and assumptions. To simulate the four major mechanisms of heat transfer, moisture transport, carbonation process, and chloride penetration, the ANSYS program has been used. For each physical environment, particular characteristics, such as geometry, element type, material properties, boundary conditions, and applied loads, are first defined. Then the procedure begins by solving all the mechanisms one-by-one at each time step. At the end of a time step, the obtained results are collected and used to update the model for the next step. One of the novelties of this procedure is that while it considers all the nonlinearities involved in each of the physical environments, their time-dependent interactions are also taken into account.

To perform transient thermal analysis in ANSYS, it is necessary to select an appropriate element type. Among various element types available in ANSYS, SOLID70 has been chosen in this study for the previously defined physical environments. According to the ANSYS Elements Reference, SOLID70 has eight nodes, each with a single degree of freedom for temperature. This element has a three-dimensional thermal conduction capability and can be used for steady-state or transient thermal analysis. By using this element type, a three-dimensional finite-element model of a concrete member is generated. As shown in Fig. 1, a typical segment of this member has a total thickness of 25 cm with the longitudinal rebars placed 20 cm center-to-center of each other. The cover depth is defined as the perpendicular distance from the center of a rebar to the concrete surface and here is assumed equal to 5 cm. This model can represent an actual bridge deck subjected to deicing salts or a RC slab of port facilities exposed to air-borne sea salts.

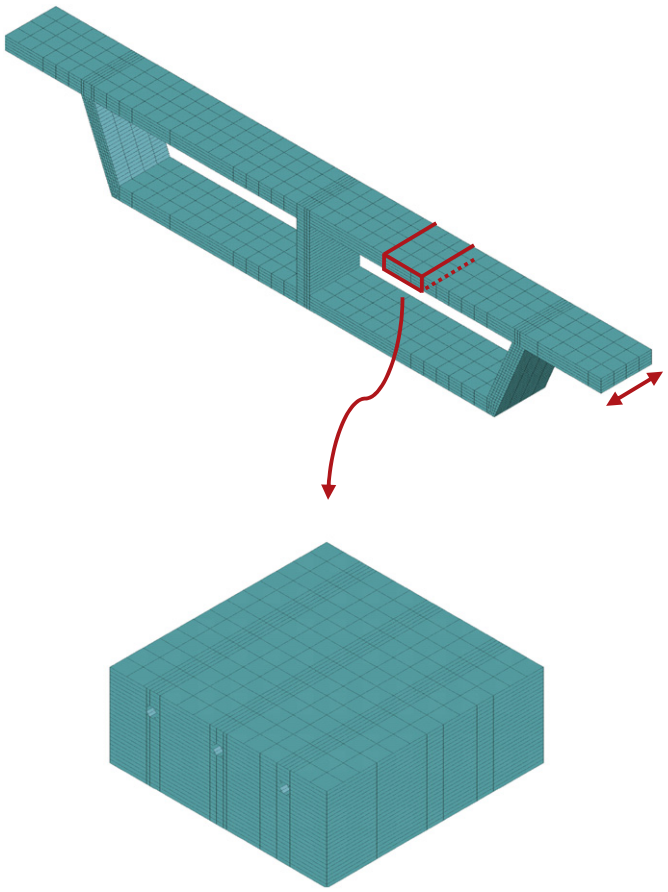

Fig. 1. Three-dimensional finite-element model of a typical reinforced concrete member (unit length).

3. Chloride intrusion into concrete

Chloride-induced corrosion is initiated by the ingress of chloride ions into the RC member during the concentration and diffusion cycles. The sources of chloride ions are mainly air-borne sea salts in coastal areas or deicing salts used over winter months. This paper focuses on the corrosion caused by the sea-salt particles floating in the air and assumes that the diffusion process is the dominant mode of chloride intrusion. To study the diffusion process, it is essential to find the change of the chloride content at different depths of the RC member. The total chloride content refers to the total acid-soluble chloride in the concrete, which is the summation of free chlorides and bound chlorides. The relationship among the total, C_t, free, C_f, and bound, C_b, chloride content in the unsaturated concrete can be described as follows [33]:

$$C_t = C_b + w_e C_f \tag{1}$$

where w_e is the evaporable water content (m^3 of evaporable water per m^3 of concrete). It should be noted that the water in the concrete is composed of evaporable water, w_e, and non-evaporable water, w_{ne}. The non-evaporable water is produced because of hydration reactions and has no effect on the transfer of chloride ions. On the other hand, the evaporable water, which is considered as the water held in concrete pores, takes part in the diffusion process as one of the internal parameters. According to [31], the evaporable water content can be calculated as the summation of the capillary pore water, w_c (m^3 of capillary pore water per m^3 of concrete), and gel pore water, w_g (m^3 of gel per m^3 of concrete), as below:

$$w_e = w_c + w_g = [(w/c - 0.36\alpha) + (0.18\alpha)]c/\gamma_w \tag{2}$$

where c is the cement content, w/c, the water-to-cement ratio, γ_w, the water density, and α, the degree of hydration. The degree of hydration can be calculated as a time-dependent parameter following the equation suggested by [18]. It should be noted that Eq. (2) is a simplified formulation only for ordinary portland cement (OPC) and it does not take into account the effects of a few parameters, such as carbonation, interfacial transition zone, non-porous aggregates, air voids, and curing conditions.

At the constant temperature of 23 °C and the water-to-cement ratio of 0.5, the change of evaporable water content with concrete age is shown in Fig. 2 for a set of cement contents ranging from 300 to 450 kg/m^3. It can be understood from this figure that the amount of evaporable water decreases during the aging process of the concrete until it reaches a constant level within less than 100 days. As a case in point, the evaporable water content for the cement content of 350 kg/m^3 experiences no change after reaching 0.136 (13.6%) within only 60 days.

According to Fick's second law, which is based on the mass conservation principle, the diffusion process is expressed as the change in the free chloride content over the time, t [25]:

$$\frac{\partial c_f}{\partial_t} = -div\left[\frac{D_{Cl}}{1 + (1/w_e)(\partial C_b/\partial C_f)}\nabla(C_f)\right] \tag{3}$$

where D_{Cl} is the chloride diffusion coefficient and $\partial C_b/\partial C_f$ is the binding capacity. The chloride binding capacity in Eq. (3) characterizes the

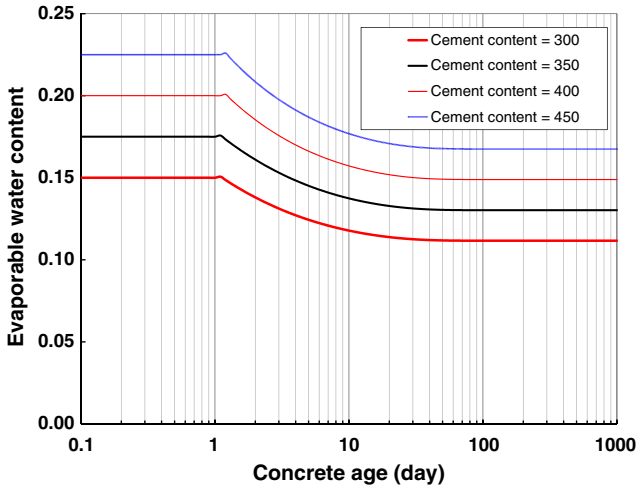

Fig. 2. Change of evaporable water content with concrete age for a range of cement contents.

relationship between the free and bound chloride ions in the concrete at a constant temperature [24]. This parameter, which is also referred to as the binding isotherm, can be calculated using one of the three equations suggested by [25]. Eqs. (4)–(6) represent the idealized binding isotherms and simulate the exposure conditions of marine structures.

(I) Linear isotherm:

$$C_b = \alpha_{lin} C_f \rightarrow \frac{\partial C_b}{\partial C_f} = \alpha_{lin} \tag{4}$$

(II) Langmuir isotherm:

$$C_b = \frac{\alpha_L C_f}{1+\beta_L C_f} \rightarrow \frac{\partial C_b}{\partial C_f} = \frac{\alpha_L}{(1+\beta_L C_f)^2}. \tag{5}$$

(III) Freundlich isotherm:

$$C_b = \alpha_F C_f^{\beta_F} \rightarrow \frac{\partial C_b}{\partial C_f} = \alpha_F \beta_F C_f^{\beta_F - 1} \tag{6}$$

where α and β are equal to 0.39 and 0.07 for the Langmuir isotherm and 1.05 and 0.36 for the Freundlich isotherm, respectively.

The chloride diffusion coefficient in Eq. (3), D_{Cl}, is calculated by taking into account the effects of all major influential parameters, such as water-to-cement ratio, ambient temperature, relative humidity, carbonation, age of the concrete, chloride content, and chloride binding capacity. The chloride diffusion coefficient can be determined from a diffusion coefficient estimated for a reference temperature and humidity, $D_{Cl,ref}$, multiplied by a series of modification factors as below:

$$D_{Cl} = D_{Cl,ref}\, F_1(T)\, F_2(H)\, F_3(\mathcal{R})\, F_4(t_e)\, F_5(C_f) \tag{7}$$

where $F_1(T)$ accounts for the dependence of chloride diffusion coefficient on the ambient temperature, $F_2(H)$ represents the influence of relative humidity, $F_3(\mathcal{R})$ evaluates the effect of carbonation process, $F_4(t_e)$ denotes the influence of concrete age, and $F_5(C_f)$ considers the effect of free chloride content on the chloride diffusion coefficient. The nonlinear time-dependent effects of the mentioned parameters on the corrosion process are discussed in detail through independent yet interacting physical environments.

The reference chloride diffusion coefficient, $D_{Cl,ref}$, is influenced by various internal parameters, such as concrete mix properties, curing conditions, and the chemical composition of steel and concrete. Among all these parameters, it has been proved that the change in concrete mix properties, and especially in the water-to-cement ratio, has a significant influence on the chloride diffusion coefficient [4,30,38]. The level of water-to-cement ratio directly affects both the capillary porosity and permeability of the concrete, which may result in significant change in the diffusion rate of chloride ions.

A number of models have been developed to study the effects of water-to-cement ratio on the chloride diffusion coefficient. As a case in point, [12] found that when the water-to-cement ratio of OPC concrete changes from 0.5 to 0.6, the $D_{Cl,ref}$ increases from 1.7 to 3.3 ($\times 10^{-8}$ cm^2/s). In the other study conducted by [29], the effects of water-to-cement ratio as well as ambient temperature on the $D_{Cl,ref}$ were examined. At the constant temperature of 23 °C, they measured the $D_{Cl,ref}$ as 2.60, 4.47, and 12.50 ($\times 10^{-8}$ cm^2/s) for the water-to-cement ratios of 0.4, 0.5, and 0.6, respectively. When common Portland cement is used, [22] suggests the following relationship for the $D_{Cl,ref}$:

$$\log\left(D_{Cl,ref}\right) = -3.9(w/c)^2 + 7.2(w/c) - 2.5 \tag{8}$$

where $D_{Cl,ref}$ is in cm^2/year. [8] updated the coefficients of the above equation with the data from some other studies considering the concrete with and without additives. The reference chloride diffusion coefficients obtained from the existing literature have been summarized in Fig. 3. Review of the available data shows a similar trend of increase in $D_{Cl,ref}$ and indicates that for the water-to-cement ratios in the common range of 0.3 to 0.6, the proposed diffusion coefficients are almost similar. In the current study, it is assumed that for a water-to-cement ratio of 0.5, the reference chloride diffusion coefficient is equal to 3.4 ($\times 10^{-8}$ cm^2/s). It should be emphasized that the reference diffusion coefficient still does not include the effects of external parameters, such as temperature, humidity, carbonation, and free chloride content. By taking into account these parameters, the $D_{Cl,ref}$ will be improved to the D_{Cl} through the next sections.

4. Ambient temperature

Ambient temperature has been identified as one of the external parameters that directly affect the diffusion process in the concrete. Based on the Arrhenius law, [33,45] proposed an influence factor to consider the effects of temperature variation on the chloride diffusion coefficient. This factor compares the current temperature, T, with a reference temperature, T_{ref}, by using Eq. (9):

$$F_1(T) = \exp\left[\frac{E}{R}\left(\frac{1}{T_{ref}} - \frac{1}{T}\right)\right] \tag{9}$$

where R is the gas constant (kJ/(mol.K)) and E is the activation energy of diffusion process (kJ/mol). According to [29], the value of E for a cement paste made of OPC depends on the water-to-cement ratio and

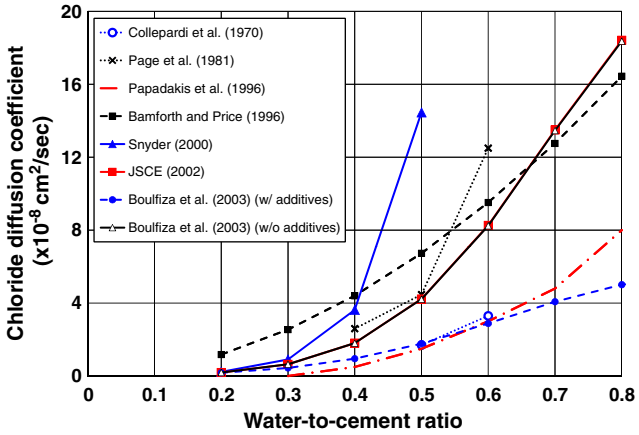

Fig. 3. Summary of suggested values for the reference chloride diffusion coefficient as a function of water-to-cement ratio.

can be considered as 41.8 ± 4.0, 44.6 ± 4.3, and 32.0 ± 2.4 (kJ/mol) for w/c of 0.4, 0.5, and 0.6, respectively. In Eq. (9), both T and T_{ref} are in K and the reference temperature is usually assumed equal to 296 K.

Since the average temperature varies within a three-dimensional concrete member, it is essential to find the expected nodal temperature at different points of the finite-element model. This will be used to determine the values of $F_1(T)$ at each time step. The governing partial differential equation for the heat flow through the concrete member is based on the principle of energy conservation and Fourier's heat conduction law. This can be written as:

$$\mathrm{div}(k_t\,\mathrm{grad}(T)) + q_t = \rho c_t \frac{\partial T}{\partial t} \tag{10}$$

where k_t is the thermal conductivity of the concrete (= 2 W/m.K), q_t, the rate of heat generation per unit volume (W/m^3), ρ, the concrete density (= 2400 kg/m^3), and c_t, the specific heat of the concrete (= 1000 J/kg.K). Considering the fact that the generation of heat during hydration process is extremely gradual and the hardened concrete does not produce or consume any major heat, the q_t is assumed to equal zero in Eq. (10). It is worth mentioning that the thermal conductivity, specific heat, and density of the concrete are dependent on the concrete mixture and its environmental conditions. However, the effects of these parameters are usually so small that they can be neglected [6,33]. As a result, the heat transfer differential equation, given in Eq. (10), can be treated as a linear problem that is solved with no need to consider the other mechanisms.

To solve the Eq. (10) as a transient field problem, the developed finite-element model of the concrete member is subjected to the transient thermal analysis using the ANSYS program. To introduce the initial and boundary conditions, the ambient temperature data should be gathered within a specific region where the RC member is located. In the current study, the daily temperature data of the Los Angeles area has been obtained for the last 15 years (1995 to 2009) from the National Oceanic and Atmospheric Administration [28]. From this database, it is evident that the recorded temperature, T_{env}, has a periodic trend over the year and a sinusoidal function can be fitted to the data:

$$T_{env}(t) = 291 - 15\sin(2\pi t/365) \tag{11}$$

where t is in days ($0 \le t \le 365$). From the sinusoidal function assigned to the local temperature data, the initial condition is defined as:

$$T(x,y,z,t=0) = T_0(x,y,z) \tag{12}$$

where $T_0(x,y,z)$ is equal to 291 K. The boundary conditions are applied to the top and bottom surfaces of the concrete member. It is assumed that the temperature at the top surface follows the trend of Eq. (11) over time. The bottom surface of the member has also the same trend with the half variation amplitude. Based on the discussed assumptions and equations, the transient thermal analysis is performed on the finite-element model to calculate the temperature distribution in the nodes and elements of the concrete member. The temperature data are stored at each time step and then used as initial conditions for the next time step of analysis. Fig. 4 shows the temperature variation at different depths of the concrete model during a 60-month period. As expected, the obtained temperature values have a similar periodic trend but with different amplitudes. It can be understood from this figure that the average of temperature inside the concrete member has a layer-by-layer variation. This directly affects the $F_1(T)$ parameter and makes it a spatial modification factor for the chloride diffusion coefficient (Fig. 5).

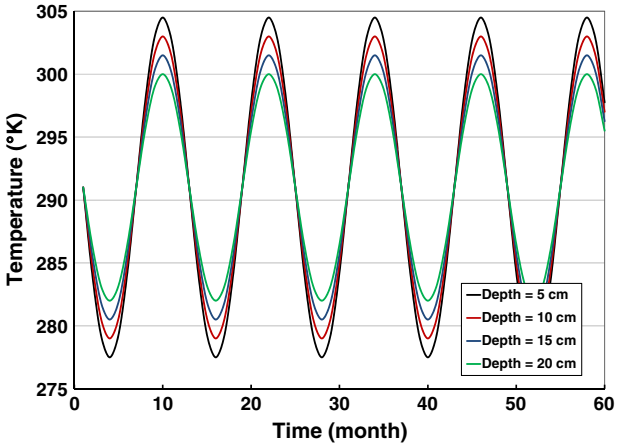

Fig. 4. Temperature variation at different depths of the concrete member during a 60-month period.

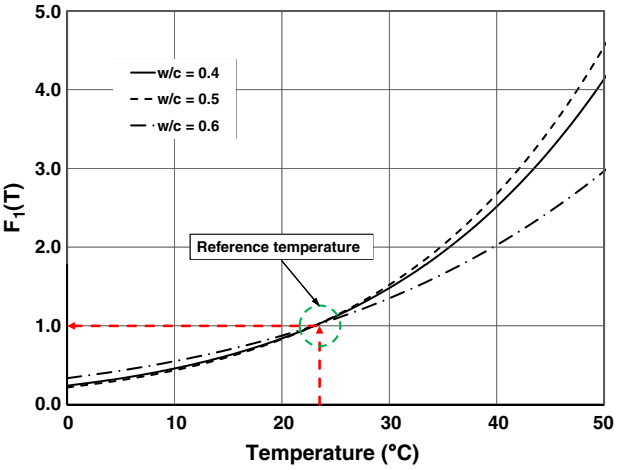

Fig. 5. Estimated values for $F_1(T)$ as a function of temperature.

5. Relative humidity

An accurate estimation of the water content of the concrete is critical for the study of chloride diffusion process. In addition to serving as a transport agent, water is an essential component of numerous chemical reactions that may cause deterioration of the concrete. The transport of water in the concrete, as a porous medium, is complicated for two major reasons: 1) a wide range of pore sizes is present in the concrete, and 2) as the concrete ages, the pore structure changes significantly due to hydration products. Different transport mechanisms, such as convection, diffusion, desorption and adsorption, and capillary suction may apply individually or simultaneously for the transport of water in the concrete.

Although depending on the pore relative humidity and microstructure of the concrete, one or more of the mentioned transport mechanisms may become dominant, [42] indicated that the diffusion process usually dominates the transport of moisture in the concrete. Based on the semi-empirical expressions proposed by [5], the following equation was used by [33] to consider the effects of relative humidity, H, on the chloride diffusion coefficient.

$$F_2(H) = \frac{1}{\left[1 + \left(\frac{1-H}{1-H_c}\right)^4\right]} \tag{13}$$

where H_c is the critical humidity level at which $F_2(H)$ equals to the average of its maximum and minimum values (usually assumed equal to 0.75). It can be understood from Eq. (13) that consideration of the relative humidity always applies a reduction factor (less than 1.0) to the chloride diffusion coefficient.

The time-dependent pore relative humidity, H, at different spots of the concrete must be calculated from the moisture diffusion process. This process can be studied in terms of relative humidity or water content. According to [5,43,44], the formulation of moisture transport is preferred to be developed in terms of relative humidity rather than water content. This is mainly because the drop in H due to self-desiccation is rather small for common water-to-cement ratios. Furthermore, when generalization to temperature variable is considered, the gradient of H can still be considered as a driving force for the diffusion process. Hence, the pore relative humidity can be obtained by solving the below nonlinear differential equation [33]:

$$\frac{\partial H}{\partial W}\,\mathrm{div}(D_H\,\mathrm{grad}(H)) + \frac{\partial H_s}{\partial t} + K_{HT}\frac{\partial T}{\partial t} + \frac{\partial H_B}{\partial t} = \frac{\partial H}{\partial t} \tag{14}$$

where W is the total water content and D_H is the humidity diffusion coefficient. There are three additional terms in Eq. (14), where: (1) $\partial H_s/\partial t$ is the change of pore relative humidity due to the self-desiccation. As mentioned earlier, this change is small and its associated term can be neglected in a normal-strength concrete; (2) $K_{HT}\partial T/\partial t$ represents the change in the humidity due to the temperature variation, considering the hydrothermal coefficient of K_{HT} (1/K). This term has also a minor contribution, which can be neglected in this study; (3) $\partial H_B/\partial t$ takes into account the amount of water liberated during the carbonation process. This term will be discussed more in the next section.

It can be understood from Eq. (14) that two parameters mainly affect the moisture transport mechanism: (1) moisture capacity, $\partial W/\partial H$, and (2) moisture diffusivity, D_H. Since these two parameters are also the major sources of nonlinearity in Eq. (14), they are further discussed to provide more detailed information about the assumptions and equations needed for the accurate modeling of the moisture transport in the concrete.

5.1. Moisture capacity

The moisture capacity is defined as the derivative of water content with respect to pore relative humidity. The relationship between water content and pore relative humidity in a constant temperature is determined by adsorption isotherms. The adsorption of water in the concrete is influenced by a number of internal parameters; especially those that contribute to the hydration process and the constitution of the pore structure. These parameters include the water-to-cement ratio, type of cement, curing condition, temperature, and added admixtures. Xi et al. [43,44] proposed an adsorption isotherm and compared the results with the available test data. Based on this isotherm:

$$W = \frac{V_m \tau k H}{(1-kH)[1+(\tau-1)kH]} \tag{15}$$

where V_m is the monolayer capacity (equal to the mass of adsorbate required to cover the adsorbent with a single molecular layer), τ, a constant that takes into account the influence of change in temperature on the adsorption isotherm, and k, another constant resulted from the assumption that the number of adsorbed layers is a finite small number [10]. Having the adsorption isotherm defined, the moisture capacity, $\partial W/\partial H$, can be obtained from the derivative of Eq. (15) as follows:

$$\frac{\partial W}{\partial H} = \frac{\tau k V_m + Wk[1+(\tau-1)kH] - Wk(1-kH)(\tau-1)}{(1-kH)[1+(\tau-1)kH]}. \tag{16}$$

The reciprocal of Eq. (16) results in $\partial H/\partial W$, which is one of the parameters required to solve Eq. (14). It can be understood from Eq. (16) that the value of $\partial H/\partial W$ is not a constant and varies as a function of temperature, humidity, and the age of the concrete [32,43,44]. This parameter is regularly updated in the developed finite-element framework to incorporate a more realistic estimate of the moisture capacity at different time steps.

5.2. Moisture diffusion coefficient

The nonlinear time-dependent variation of the humidity diffusion coefficient can be evaluated using a multi-factor equation introduced by [5] as:

$$D_H = D_{H,ref} F_{H1}(T) F_{H2}(H) F_{H3}(t_e) F_{H4}(\mathcal{R}) \tag{17}$$

where $F_{H1}(T)$ accounts for the dependence of the humidity diffusion coefficient on the ambient temperature, $F_{H2}(H)$ represents the influence of relative humidity, $F_{H3}(t_e)$ denotes the influence of concrete age, and $F_{H4}(\mathcal{R})$ considers the effect of carbonation process on the humidity diffusion coefficient. In Eq. (17), $D_{H,ref}$ is the reference humidity diffusion coefficient calculated at the standard temperature and humidity. Based on the experimental data provided by Federal Polytechnic of Zurich, [35] studied the humidity diffusion coefficient as a function of water-to-cement ratio. For a concrete with the water-to-cement ratio of 0.5, they suggest a reference diffusion coefficient of 2.0×10^{-11} m^2/s. This value is in good agreement with the results of similar studies by [5,19], and the most recent [11].

The effect of ambient temperature on the humidity diffusion coefficient, $F_{H1}(T)$, is taken into account by using Eq. (9). The only difference is that the activation energy, E, needs to be changed to 22.0 (kJ/mol) for the moisture transport [29]. For the humidity modification factor, $F_{H2}(H)$, the following empirical formula has been proposed [44]:

$$F_{H2}(H) = \alpha_H + \beta_H\left[1-2^{-10^{\gamma_H(H-1)}}\right] \tag{18}$$

where α_H, β_H, and γ_H are coefficients calibrated from the test data. In Eq. (18), α_H represents the lower bound of the modification factor approached at the low humidity level. The $\beta_H/2$ is the increment from the low humidity level to saturation state, and γ_H characterizes the humidity level at which the modification factor begins to increase. These parameters are majorly affected by the water-to-cement ratio. The porosity of concrete increases when a higher water-to-cement ratio is used. Hence, the volume fraction of macro pores increases as well, which causes a faster migration of water molecules in the low humidity level. As a result, α_H and γ_H are expected to have larger values with the increase in water-to-cement ratio. On the other hand, β_H first increases with water-to-cement ratio for the same reason mentioned earlier, but after reaching a certain water-to-cement ratio, it starts dropping. This is due to the fact that the increase of diffusivity from a low humidity level to saturation state will be slowed down by the increase in the volume fraction of macro pores. Based on the equations suggested by [44], the effects of water-to-cement ratio on α_H, β_H, and γ_H are shown in Fig. 6. Furthermore, Fig. 7 depicts the variation of $F_{H2}(H)$ as a function of the relative humidity for a range of water-to-cement ratios.

In Eq. (17), $F_{H3}(t_e)$ is to consider the effect of age of the concrete. The aged concrete is hydrated and its porous area decreases. This causes a reduction of the moisture diffusion coefficient as a function of time. According to [40], the below formula can be used to calculate this modification factor:

$$F_{H3}(t_e) = \chi + (1-\chi)\left(\frac{28}{t_e}\right)^{0.5} \tag{19}$$

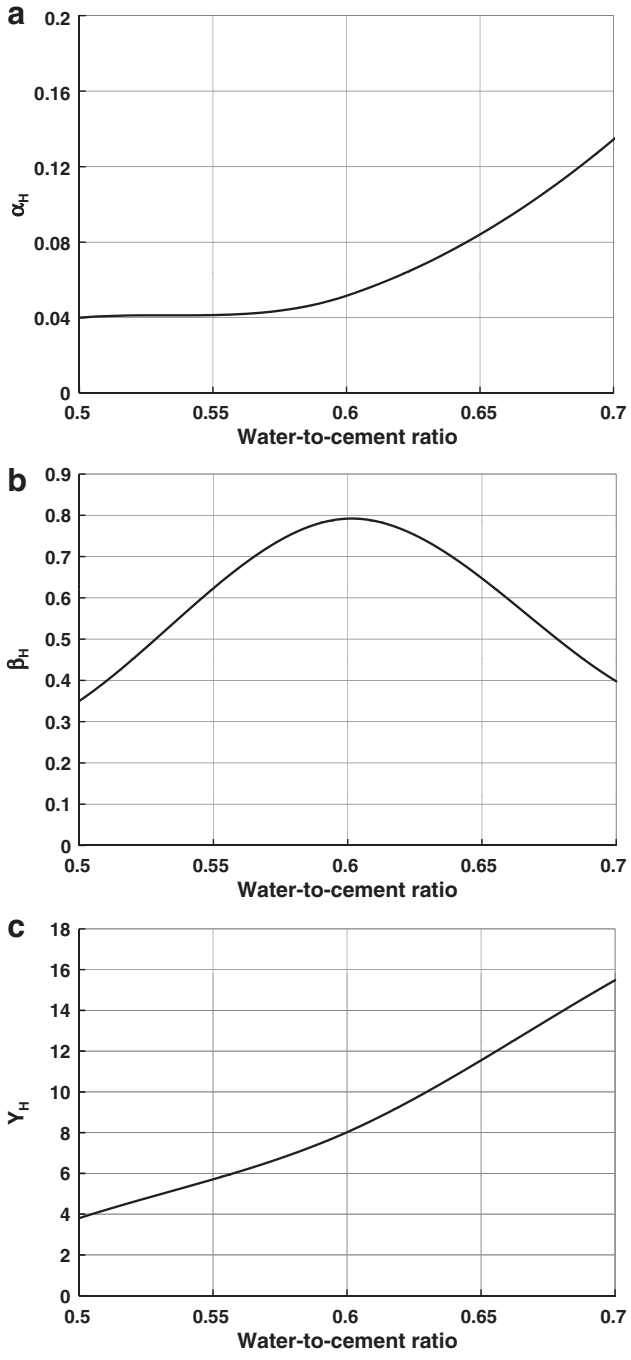

Fig. 6. Effects of water-to-cement ratio on α_H, β_H, and γ_H.

where t_e is the age of the concrete (day) and χ is the ratio of the diffusivity at the time of infinity to the diffusivity after 28 days. The effect of age on the diffusion of moisture is shown in Fig. 8 for different χ values. The last modification factor of Eq. (17), $F_{H4}(\mathcal{R})$, is to consider the effect of those chemical reactions that result in precipitation (like the generation of water during the carbonation process). The precipitation reduces the humidity diffusion coefficient following the below equation proposed by [33]:

$$F_{H4}(\mathcal{R}) = 1 - \zeta\mathcal{R} \tag{20}$$

where the value of ζ ranges between 0 and 1. If the diffusion process results in no reduction in porosity, ζ would become zero. The $\mathcal{R}$ parameter will be discussed later in the carbonation section.

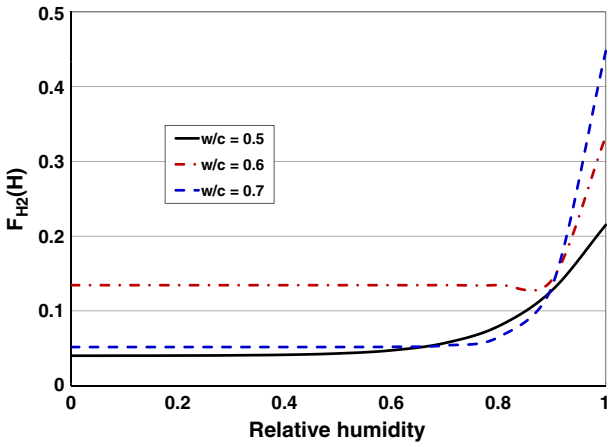

Fig. 7. Variation of $F_{H2}(H)$ as a function of the relative humidity for a range of water-to-cement ratios.

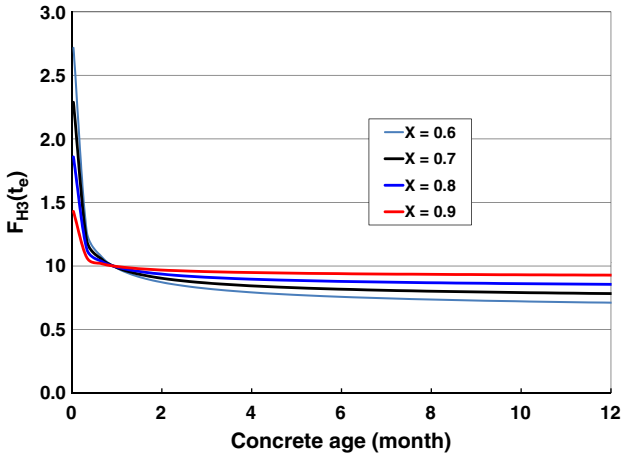

Fig. 8. Change of $F_{H3}(t_e)$ with the age of the concrete.

Considering all the mentioned equations and coefficients, the moisture transport mechanism in the concrete is simulated by using the transient thermal analysis of the ANSYS program. For this purpose, the thermal parameters required for the analysis are interpreted as their analogous moisture parameters following Eq. (14). Similar to the transient field defined for the ambient temperature, the relevant coefficients for the moisture transport mechanism need to be identified and introduced. Comparing Eq. (14) with Eq. (10) indicates that the moisture capacity, $\partial W/\partial H$, can be mapped to the specific heat capacity, c_t, while the humidity diffusion coefficient, D_H, is equivalent to the thermal conductivity, k_t. The humidity generated due to the carbonation process, $\partial H_c/\partial t$, is also mapped to the rate of heat generation, q_t, using the body force option available in ANSYS.

Before solving the transient field problem, the initial and boundary conditions are determined. Similar to the ambient temperature, the local humidity information is obtained to be used in the finite-element model. In this study, the average monthly relative humidity data for the Los Angeles area has been collected to find the annual trend of the relative humidity. Review of available data indicates that the recorded relative humidity, H_{env}, is periodic in nature and is repeated throughout the years as below:

$$H_{env} = 0.65 + 0.13\sin(\pi t/365) \tag{21}$$

where t is in days ($0 \le t \le 365$). From the sinusoidal function assigned to the local relative humidity data, the initial condition is defined as:

$$H(x,y,z,t=0) = H_0(x,y,z) \tag{22}$$

where $H_0(x,y,z)$ is equal to 0.65. The boundary conditions are applied to the top and bottom surfaces of the concrete member. The relative humidity at both surfaces has identical variation following the trend of Eq. (21) over time.

As previously explained, the key parameters of the moisture transport mechanism, such as moisture capacity and humidity diffusion coefficient, are functions of a number of nonlinear time-dependant parameters, including: concrete properties, ambient temperature, pore relative humidity, exposure time, and carbonation process. Hence, the finite-element model needs to be subjected to a series of transient thermal analysis. At each time step, the data required from the other physical environments are obtained and used to update the moisture capacity, humidity diffusion coefficient, and the rate of humidity generation. By using this procedure, the simultaneous effects of various stressors along with their mutual interactions are fully investigated.

Based on the discussed assumptions and equations, the transient thermal analysis is performed on the three-dimensional model of the concrete member to find the humidity distribution over the nodes and elements of the member. The humidity data are stored at each time step and then used as initial conditions for the next time step of analysis. Fig. 9 depicts the expected change in the pore humidity level at different depths of the concrete model during a 50-year period. It can be seen from this figure that the pore relative humidity varies from one layer to another one, demonstrating the effects of moisture diffusivity on the pore humidity. As it is evident in Fig. 9, there is a periodic fluctuation in the pore humidity curves, which is due to the periodic trend of the surrounding relative humidity. Fig. 10 shows the humidity diffusion coefficient estimated at different depths of the concrete model over 30 years. As mentioned earlier, since various parameters affect this coefficient and all these parameters have different spatial values, a location-dependent estimate of the humidity diffusion coefficient is necessary to obtain more realistic results for the pore humidity distribution.

6. Carbonation process

In urban and industrial regions, the concentration of carbon dioxide, CO_2, produced by various environmental pollutants is the main cause of the carbonation process in the RC members. During this process, the chemical reactions between carbon dioxide and cement

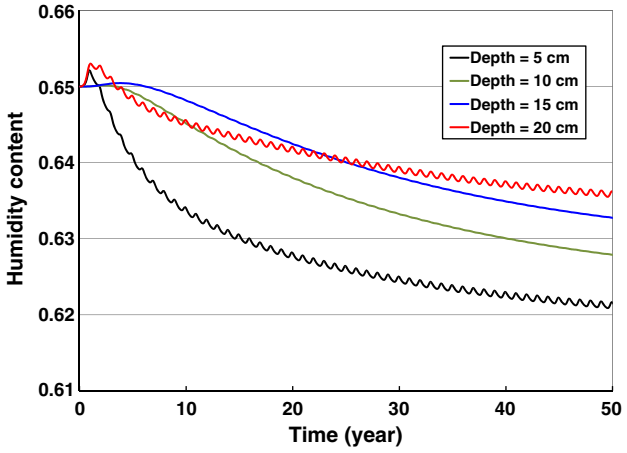

Fig. 9. Pore humidity content at different depths of the concrete model during a 50-year period.

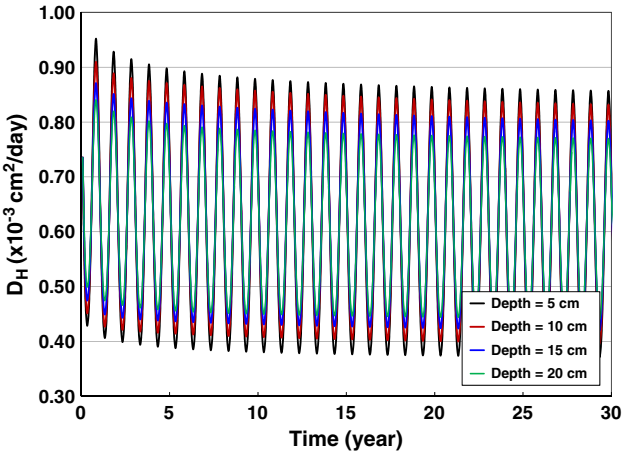

Fig. 10. Humidity diffusion coefficient estimated at different depths of the concrete model during a 30-year period.

hydration products result in the reduction of the alkalinity of the concrete, which by itself adversely affects the ability of the concrete to protect the steel rebars from corrosion. During the hydration process of OPC concrete, the calcium oxide in cement, CaO, forms the calcium silicate hydrate, C–S–H, and calcium hydroxide, $Ca(OH)_2$. The presence of the calcium hydroxide and other alkalis in the intact concrete provides a pH of greater than 12.4. However, when CO_2 penetrates into the concrete, it dissolves in the concrete pore water and forms the carbonic acid. The carbonic acid reacts with the alkaline hydration products and reduces the pH of the concrete to below 9.0. At this point, the passivating film around the steel rebar is eliminated and it becomes exposed to the oxygen and chloride ion bearing solution. This process, which facilitates the onset of corrosion, is called carbonation and can be expressed as [30]:

$$Ca(OH)_2 \rightarrow Ca^{2+} + 2OH^- \tag{23}$$

$$H_2O + CO_2 \rightarrow HCO_3^- + H^+ \rightarrow CO_3^{2-} + 2H^+ \tag{24}$$

$$Ca^{2+} + 2OH^- + CO_3^{2-} + 2H^+ \rightarrow CaCO_3 + 2H_2O \tag{25}$$

From the reaction of carbon dioxide, CO_2, with calcium hydroxide, $Ca(OH)_2$, in the hardened cement paste, the calcium carbonate, $CaCO_3$, is produced. Since the calcium carbonate is not soluble in the pore water, it precipitates in the pore area and decreases the pore volume of the OPC concrete. This will change the transport properties and permeability of the concrete [20,21]. It is worth mentioning that the described reactions ideally occur in a humidity range of 50% to 70%. In the humidity levels of less than 50%, CO_2 ions cannot be completely dissolved due to the inadequate water in the pores. On the other hand, in the humidity levels of higher than 70%, the water in pore volume inhibits the CO_2 diffusion and causes lower rates of carbonation [21,27,30].

Since the carbonation process is affected by a number of nonlinear time-dependent parameters, the capabilities of the developed finite-element framework are used to determine the CO_2 content and the degree of carbonation at various points of the three-dimensional model. The governing equation to simulate the transport of CO_2 in the concrete is based on Fick's second law and can be written as:

$$\mathrm{div}(D_B\,\mathrm{grad}(B)) + q_b = \frac{\partial B}{\partial t} \tag{26}$$

where D_B is the CO_2 diffusion coefficient (m^2/s), B, the pore CO_2 concentration (kg/m^3 of pore solution), and q_b, the sink term representing the rate of CO_2 consumption during the carbonation reactions. In

Eq. (26), the CO_2 diffusion coefficient is a function of both internal and external parameters. Hence, [34] introduced a multi-factor equation to consider the effects of major influential parameters, including: ambient temperature, $F_{B1}(T)$, relative humidity, $F_{B2}(H)$, age of the concrete, $F_{B3}(t_e)$, and change of the concrete pore structure during the carbonation process, $F_{B4}(\mathcal{R})$.

$$D_B = D_{B,ref} F_{B1}(T) F_{B2}(H) F_{B3}(t_e) F_{B4}(\mathcal{R}) \tag{27}$$

where $D_{B,ref}$ is the reference CO_2 diffusion coefficient in the controlled temperature and humidity conditions. There are a few equations available in the literature to determine the $D_{B,ref}$ as a function of concrete properties (e.g., [11,30]). According to the [11], the reference CO_2 diffusion coefficient for a normal strength concrete in the standard temperature and relative humidity of 65% can be calculated as:

$$D_{B,ref} = D_{B0} 10^{-0.05 f'_{cm}} \tag{28}$$

where f'_{cm} is the mean value of the 28-day compressive strength of the concrete (MPa) and D_{B0} is equal to $10^{-6.1}$ m^2/s. Hence, for a concrete with 40 MPa compressive strength, the $D_{B,ref}$ becomes equal to 7.94×10^{-9} m^2/s. In Eq. (27), $F_{B1}(T)$, $F_{B3}(t_e)$, and $F_{B4}()$ can be estimated following the formulas given in Eqs. (9), (19), and (20), respectively. Furthermore, $F_{B2}(H)$ is calculated as [34]:

$$F_{B2}(H) = (1-H)^{2.5} \tag{29}$$

where H is the corresponding pore relative humidity.

In addition to the CO_2 diffusion coefficient, the sink term of Eq. (26), q_b, needs to be defined. This term indicates the consumption rate of the carbon dioxide during the carbonation process and can be derived from the chemical and thermo-dynamic balance of the pore solution [33]. According to [9,19], the rate of CO_2 consumption during the carbonation reactions is obtained from a multi-factor equation:

$$q_b = \alpha_1 \alpha_2 f_1(H) f_2(T) f_3(\mathcal{R}) f_4(B) \tag{30}$$

where α_1 represents the reference rate at which the carbonation reaction takes place in ideal conditions. According to [35], the increase of this coefficient reduces the estimated carbonation depth, but since the influence of this coefficient on the final result is less than 2%, the variability of this coefficient can be deemed negligible. For the standard concrete, this coefficient is assumed equal to 2.8×10^{-7}/s [36,39]. Furthermore, α_2 is a coefficient that depends on the chemical reactions of the carbonation process. [35] showed that by increasing this coefficient the carbonation depth decreases. They have also stated that for the concrete with standard characteristics, α_2 can be assumed between 0.4 and 1.0.

There are four modification factors introduced in Eq. (30). The $f_1(H)$ and $f_2(T)$ take into account the effects of relative humidity, H, and ambient temperature, T, respectively. These two terms are calculated following Eqs. (31) and (32):

$$f_1(H) = \begin{cases} 0 & 0.0 \le H \le 0.5 \\ 2.5(H-0.5) & 0.5 \le H \le 0.9 \\ 1.0 & 0.9 \le H \le 1.0 \end{cases} \tag{31}$$

$$f_2(T) = A \exp\left(-\frac{E_0}{RT}\right) \tag{32}$$

where A is a constant assumed equal to 3.6×10^{10}/h and E_0 is equal to 2.08×10^6 N.m/kg. The third modification factor, $f_3(\mathcal{R})$, is to account for the reduction in the concrete porosity due to carbonation products. This reduction can be considered as:

$$f_3(\mathcal{R}) = 1-\mathcal{R}^m \tag{33}$$

where m is a constant assumed equal to 1.0 and $\mathcal{R}$ is the degree of carbonation. The degree of carbonation is determined as the ratio of accumulated CO_2 already reacted with $Ca(OH)_2$ to the maximum possible concentration of reacted CO_2 in the concrete. Experimental tests on the carbonated OPC show that the capacity of the concrete for the concentration of reacted CO_2 can be estimated as a function of the cement content and concentration of CaO in the cement [39].

The last term in Eq. (30) is the $f_4(B)$ and represents the availability of CO_2 in the concrete for the carbonation process. This factor ranges between 0 for the cases with no CO_2 penetration and 1 for the cases that CO_2 concentration is on the maximum level equal to the atmospheric concentration, $[CO_2]_{env}$. Depending on the CO_2 content at different depths of the three-dimensional model, this modification factor can be calculated as:

$$f_4(B) = \frac{CO_2}{[CO_2]_{env}}. \tag{34}$$

As stated earlier in the moisture transport mechanism, the carbonation reactions also result in the generation of water. This phenomenon was introduced into the moisture transport model (Eq. (14)) using $\partial H_B/\partial t$. The equation given in [35] calculates this term as follows:

$$\frac{\partial H_B}{\partial t} = \alpha_1 \alpha_3 f_1(H) f_2(T) f_3(\mathcal{R}) f_4(B) \tag{35}$$

where all the modification factors are similar to those included in Eq. (30). The only different coefficient in Eq. (35) is α_3, which is assumed equal to 0.0017 according to [35].

Based on the explained procedure for the calculation of the parameters of Eq. (26), the physical carbonation process is simulated in the ANSYS program as a transient thermal problem. The thermal parameters required for the analysis are obtained from their analogous carbonation parameters following Eq. (26). Comparing the heat transfer model with the carbonation governing equation, it is found that while the material density, ρ, and specific heat capacity, c_t, need to be equal to 1, the thermal conductivity, k_t, and the heat generation rate, q_t, are replaced with the CO_2 diffusion coefficient, D_B, and the CO_2 consumption rate, q_b, respectively. Since both the diffusion coefficient and consumption rate highly depend on the state of carbonation, it is required to update the model parameters at each time step considering all the nonlinearities and time-dependent characteristics of the influential factors.

For the initial condition of the transient field problem, it is assumed that the concentration of CO_2 inside the three-dimensional model is zero before the analysis starts. Furthermore, a constant CO_2 concentration is assigned to the top surface of the model as the boundary condition. This boundary condition represents the atmospheric concentration of carbon dioxide, $[CO_2]_{env}$, and it is assumed equal to 0.0012 kg/m^3 of concrete. Given the initial and boundary conditions, the transient thermal analysis is performed on the three-dimensional model of the concrete member to find the concentration of CO_2 over the nodes and elements of the member. The CO_2 content data are stored at each time step and then used as initial conditions for the next time step of analysis.

Fig. 11 demonstrates the expected change in the CO_2 content at different depths of the concrete model during a 50-year period. Similar to the moisture transport mechanism, there is a variation of CO_2 content from one layer to another one because of the diffusion characteristics. Furthermore, a periodic fluctuation is observed in the CO_2 content at any given depth. This is due to the periodic trend of the external parameters like ambient temperature and relative humidity. The CO_2 diffusion coefficient estimated at different depths of the concrete model is shown in Fig. 12 for the same period of 50 years. Since the diffusion coefficient is also a function of various internal and external parameters, both spatial and temporal variability of this parameter are taken into account through the proposed procedure.

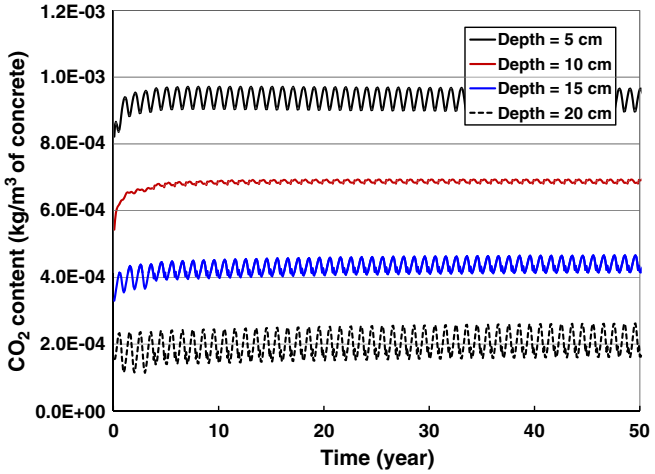

Fig. 11. Expected change in the CO_2 content at different depths of the concrete model during a 50-year period.

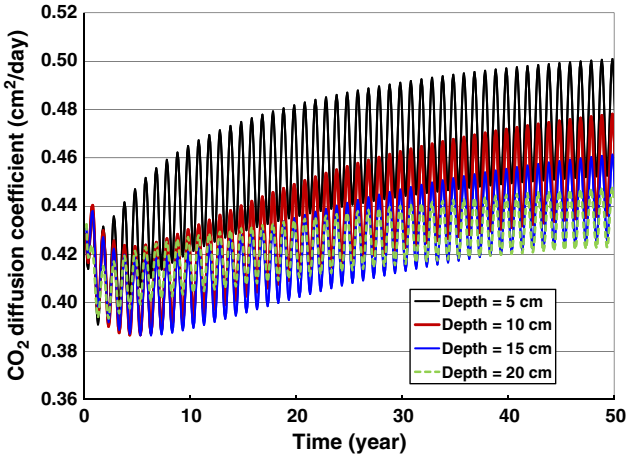

Fig. 12. CO_2 diffusion coefficient estimated at different depths of the concrete model.

7. Estimation of chloride content and corrosion initiation time

Considering the discussed methodology for the transient thermal analysis, the governing equation for the chloride diffusion process (Eq. (3)) can be rewritten as:

$$\mathrm{div}\left(D_{\mathrm{Cl,diff}}\,\mathrm{grad}\left(C_f\right)\right)=\frac{\partial C_f}{\partial t} \tag{36}$$

where $D_{\mathrm{Cl,diff}}$ is a function of the evaporable water content, chloride binding capacity, and chloride diffusion coefficient. All these parameters were explained in the previous sections and it was shown that they introduce nonlinear time-dependent characteristics to the process. As a case in point, the chloride diffusion coefficient, D_{Cl}, is modified by a number of influential parameters according to Eq. (7). The modification factors of this equation are calculated from Eqs. (9), (13), and (20) for the ambient temperature, relative humidity, and carbonation process, respectively. Furthermore, two last terms of Eq. (7) can be obtained from:

(I) *Age of Concrete*:
Concrete aging may cause a reduction in the chloride diffusion coefficient. Due to the progress of hydration reactions with time, the porosity of cement decreases. This slows down the diffusion process, especially during the initial life of the concrete. According to [25], the effect of age of the concrete on the chloride diffusion coefficient, $F_4(t_e)$, is estimated as:

$$F_4(t_e)=\left(\frac{t_{\mathrm{ref}}}{t}\right)^r \tag{37}$$

where t_{ref} is the reference time (equal to 28 days), and r, the empirical age factor assumed to equal 0.04.

(II) *Free Chloride Content*:
In spite of the consideration of free chloride content in the calculation of the chloride binding capacity, some studies consider the effect of free chloride content on the chloride diffusion coefficient [23,45]. This modification factor can be expressed as:

$$F_5(C_f)=1-\kappa(C_f)^n \tag{38}$$

where κ and n are empirical parameters, equal to $\sqrt{70}$ and 0.5, respectively. Based on Eq. (38), the time-dependent free chloride content is directly related to the diffusion coefficient and needs to be updated during the diffusion process at desired time steps.

The chloride diffusion process is simulated by using the transient thermal analysis of the ANSYS program. For this purpose, the thermal parameters required for the analysis are interpreted as their analogous chloride diffusion parameters following Eq. (36). This equation indicates that the $D_{\mathrm{Cl,diff}}$ is equivalent to the thermal conductivity, k_t, while the material density, ρ, and specific heat capacity, c_t, are assumed equal to 1. It is also worth mentioning that the heat generation rate, q_t, is equal to zero because there is no source of generation or consumption of the chloride ions in the concrete mixture.

At the beginning of analysis ($t=0$), the free chloride content within the entire depth of the three-dimensional model is considered to be zero. This is valid by assuming that no chlorides have been added to the concrete mixture. The boundary condition is applied to the top surface of the model where C_s is the surface chloride content. The surface chloride content may depend on various parameters, such as the location of the structure, orientation of its surface, chloride concentration in the environment, and the general conditions of exposure to the rain and wind [7].

According to [17,25], a surface chloride content of 17.7 kg/m^3 (of pore solution) simulates the complete submersion in seawater while this value increases to 90 kg/m^3 (of pore solution) for tidal or splash zones. The surface chloride content due to the sea salt spray has a smaller value and can be assumed as a function of distance from the coastline. Based on a field study on a group of 1158 bridges, [26] suggested a range of 0.03 to 2.95 kg/m^3 (of concrete) for surface chloride content at bridges located in the coastal zones. [41] also collected a set of data from the Mediterranean coasts and indicated a surface chloride content of 7 kg/m^3 (of concrete) for structures located on the coast. For the present paper, it is assumed that the structures under study are located at a close distance from the coast and the sea salt spray is the only mode of exposure to chloride ions. As a result, the surface chloride content has been taken equal to 3.5 kg/m^3 (of concrete). It should be noted that although a constant value for the surface chloride content has been used in this study, the developed framework is capable of considering the temporal and spatial variation of this parameter.

Based on the discussed initial and boundary conditions, the transient field problem is solved at each time step to determine the free chloride content at various depths of the three-dimensional model. During each time step, the transient analyses for heat transfer, moisture transport, and carbonation process are also conducted to update the parameters of the chloride diffusion process before the next step. Within a 50-year period, the extent of chloride penetration into the concrete has been demonstrated in Fig. 13. Furthermore, changes of the free chloride content and chloride diffusion coefficient at different depths of the model have been illustrated in Figs. 14 and 15, respectively. As expected, the chloride content has a layer-by-layer variation

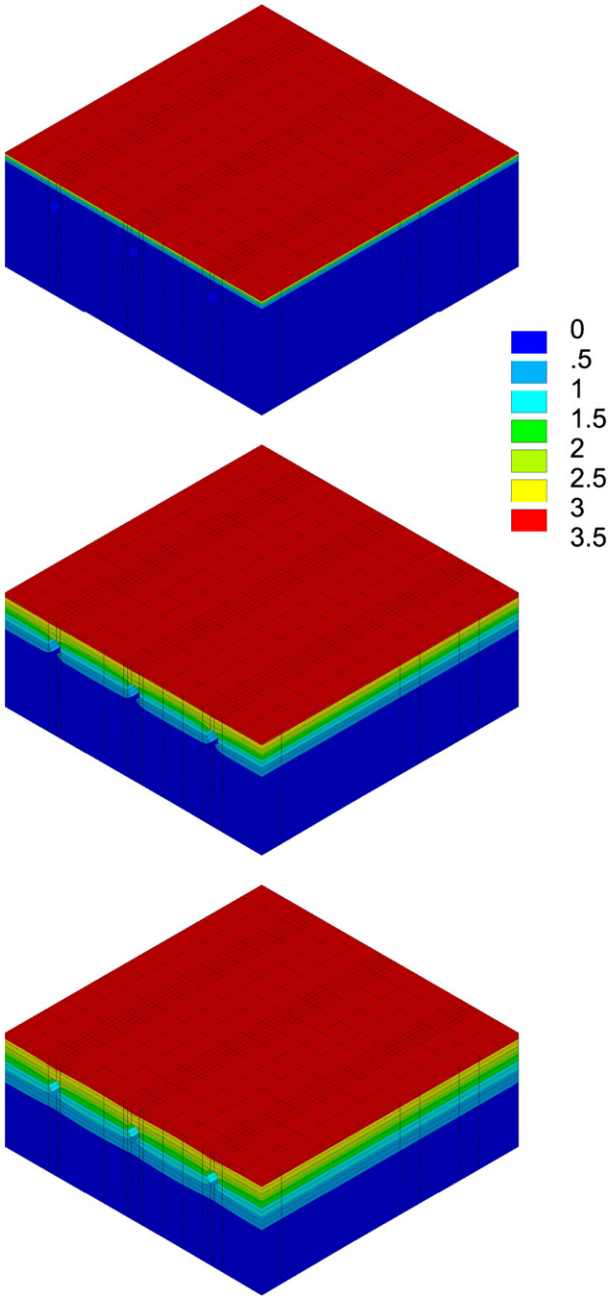

Fig. 13. Extent of chloride penetration into the concrete member after 1, 25, and 50 years.

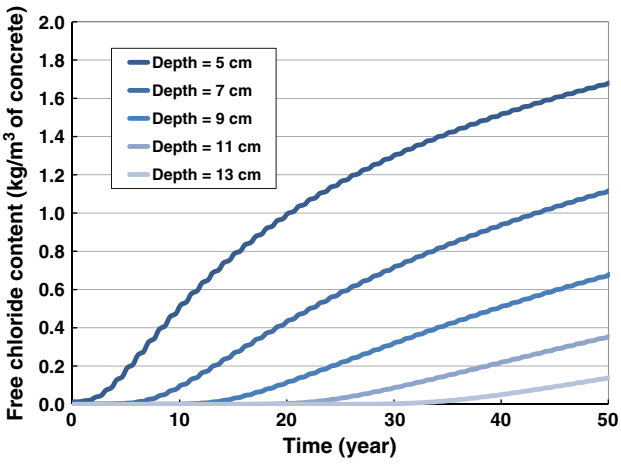

Fig. 14. Change of the free chloride content at different depths of the concrete model.

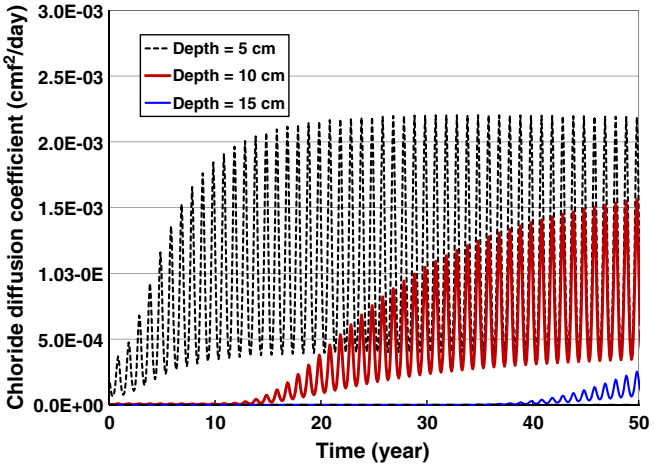

Fig. 15. Chloride diffusion coefficient estimated at different depths of the concrete model.

while there is a minor fluctuation in the calculated chloride content at any specific depth [37].

Using the binding isotherms introduced earlier, the total chloride content can be obtained from the calculated free chloride content (Eqs. (1) and (4)–(6)). The total chloride content at different time steps is used to estimate the corrosion initiation time, t_{ini}. The corrosion initiation time is determined as the time when the chloride concentration near the steel rebars reaches the threshold chloride concentration. This means:

$$C_t(t_{ini}, d_c) = C_{critical} \tag{39}$$

where d_c is the depth at which the rebars are placed (usually equal to the concrete cover depth). In Eq. (39), the $C_{critical}$ is the threshold chloride concentration causing depassivation of the concrete protection film and initiation of the corrosion process. There have been a number of research efforts during the past three decades to determine an appropriate threshold for the critical chloride content based on the corrosion science parameters [3]. Fig. 16 demonstrates a summary of data available in the literature regarding the measured or suggested values for the critical chloride concentration. For this study, the critical chloride concentration is considered to be 1% of the cement weight, which is assumed as equal to 350 kg/m^3.

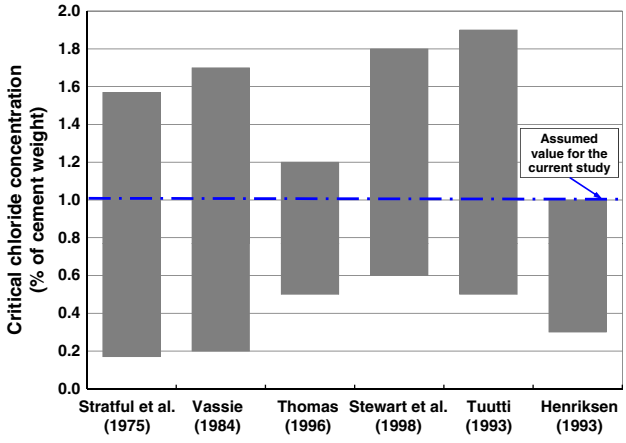

Fig. 16. A summary of data available in the literature for the critical chloride concentration.

The profiles of the total chloride content given in Fig. 17 can be used to evaluate the corrosion initiation time. Assuming the threshold value as 3.5 kg/m^3 (1% of cement weight), the initiation time is estimated as 20 years given that there are adequate corrosion conditions. To evaluate the effect of the concrete cover depth on the corrosion initiation time, different cover depths of 40, 50, and 60 mm are considered in this study resulting in a corrosion initiation time of 13.9, 23.2, and 34.8 years, respectively (Fig. 17). It is found that the corrosion initiation times obtained from the developed framework lie well within the observed range of initiation times for similar cases [23]. Considering the fact that the structural degradation mainly occurs after the corrosion initiation, a more realistic estimation of the corrosion initiation time improves the accuracy of the performance assessment of RC members over their life-cycle. Furthermore, since the calculation of the chloride content has been performed considering all the nonlinear time-dependent characteristics of the corrosion process, the developed framework can be further used to assess the actual extent of degradation as a function of time.

8. Conclusions

This paper provides an integrated finite-element framework for the prediction of corrosion initiation in reinforced concrete members subjected to environmental stressors. It has been proven that the penetration of corrosive agents into the concrete is affected by a number of internal and external parameters. The influential parameters related to the concrete properties and diffusion characteristics are categorized as internal parameters, while the ambient temperature, relative humidity, and concentration of carbon dioxide and chloride ions are considered as external parameters. Further investigation of these parameters indicates that most of them have nonlinear time-dependent characteristics and it is necessary to consider their mutual interactions in the corrosion process.

Based on a comprehensive study of available literature and resources, the current paper discusses the internal and external parameters in detail and incorporates both of them into the developed finite-element framework. This framework utilizes transient thermal analysis to simulate the four major mechanisms of heat transfer, moisture transport, carbonation process, and chloride penetration. To analyze these mechanisms, a coupled multi-physical environment is defined to call each of the physical environments in turn. The time-dependant initial and boundary conditions are applied at each time step and the transient analysis is performed on the three-dimensional finite-element model. The obtained results are stored at the end of each step and the model properties are updated for the next set of analysis. The proposed methodology calculates the spatial and temporal distributions of temperature, relative humidity, carbon dioxide and chloride content within the entire model. This is achieved while particular characteristics of various physical environments along with their mutual correlations are all taken into account.

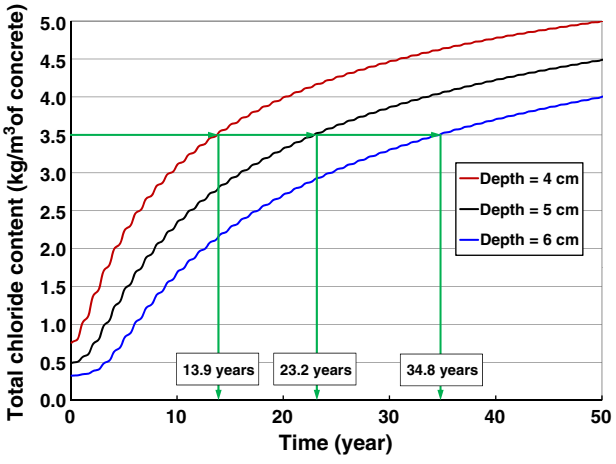

Fig. 17. Profiles of total chloride content at different cover depths of 40, 50, and 60 mm.

While the assumptions and equations given in this paper are supported by the literature, each of the explained physical environments can be further customized by complementary experimental data collected for a specific structure/region. This makes the developed framework general and adjustable for various exposure conditions. The framework proposed in this study is directly used to obtain a more accurate estimation of the chloride content and corrosion initiation time in a reinforced concrete member. This study can also be extended to evaluate the extent of structural degradation or crack propagation in reinforced concrete structures subjected to multiple environmental stressors.

References

[1] A. Alipour, B. Shafei, M. Shinozuka, Capacity loss evaluation of reinforced concrete bridges located in extreme chloride-laden environments, Journal of Structure and Infrastructure Engineering (2010), doi:10.1080/15732479.2010.525243.
[2] A. Alipour, B. Shafei, M. Shinozuka, Performance evaluation of deteriorating highway bridges in high seismic areas, ASCE Journal of Bridge Engineering 16 (5) (2011) 597–611.
[3] U. Angst, B. Elsener, C.K. Larsen, P. Vennesland, Critical chloride content in reinforced concrete — a review, Journal of Cement and Concrete Research 39 (12) (2009) 1122–1138.
[4] P.B. Bamforth, W.F. Price, An International Review of Chloride Ingress into Structural Concrete. Rep. No. 1303/96/9092, Taywood Engineering Ltd., Technology division, Middlesex, U.K, 1996.
[5] Z.P. Bazant, L.J. Najjar, Nonlinear water diffusion in unsaturated concrete, Journal of Materials and Structures 5 (25) (1972) 3–20 Paris, France.
[6] Z.P. Bazant, W. Thonguthai, Pore pressure and drying of concrete at high temperature, Journal of the Engineering Mechanics Division IM(EM5) (1978) 1059–1079.
[7] L. Bertolini, Steel corrosion and service life of reinforced concrete structures, Journal of Structure and Infrastructure Engineering 4 (2) (2008) 123–137.
[8] M. Boulfiza, K. Sakai, N. Banthia, H. Yoshida, Prediction of chloride ions ingress in uncracked and cracked concrete, ACI Materials Journal (2003) 38–48 Title No. 100-M5.
[9] L. Breiger, F.H. Wittmann, Numerical simulation of carbonation of concrete, Material and Science Restoration, Tech. Akad. Esslingen, Ostfildern, 1986.
[10] S. Brunauer, J. Skalny, E.E. Bodor, Adsorption on nonporous solids, Journal of Colloid Interface Science 30 (4) (1969) 546–552.
[11] CEB-FIP Bulletin 55, Model Code, 2010 federation internationale du béton (fib).
[12] M. Collepardi, A. Marciallis, R. Turriziani, Kinetic of penetration of chloride ions into concrete, Industria Italiana del Cemento 4 (1970) 157–164.
[13] Y.G. Du, L.A. Clark, A.H.C. Chan, Residual capacity of corroded reinforcing bars, Magazine of Concrete Research 57 (3) (2005) 135–147.
[14] Y.G. Du, L.A. Clark, A.H.C. Chan, Effect of corrosion on ductility of reinforcing bars, Magazine of Concrete Research 57 (7) (2005) 407–419.
[15] T. El Maaddawy, K. Soudki, A model for prediction of time from corrosion initiation to corrosion cracking, Journal of Cement and Concrete Composites 29 (3) (2007) 168–175.
[16] C. Fang, K. Lundgern, M. Plos, K. Gylltoft, Bond behavior of corroded reinforcing steel bars in concrete, Journal of Cement and Concrete Composites 36 (10) (2006) 1931–1938.
[17] G.K. Glass, N.R. Buenfeld, The influence of chloride binding on the chloride induced corrosion risk in reinforced concrete, Journal of Corrosion Science 42 (2) (2000) 329–344.
[18] S.H. Han, Influence of diffusion coefficient on chloride ion penetration of concrete structures, Journal of Construction and Building Materials 21 (2) (2007) 370–378.
[19] Y.F. Houst, P.E. Roelfstra, F.H. Wittmann, A model to predict service life of concrete structures, Proceedings of International Colloquium on Material Science and Restoration, Ed. Lack and Chemie, Filderstadt, 1983, pp. 181–186.
[20] O.B. Isgor, A.G. Razaqpur, Finite element modeling of coupled heat transfer, moisture transport and carbonation processes in concrete structures, Journal of Cement and Concrete Composites 26 (1) (2004) 57–73.
[21] B.F. Johanesson, Nonlinear transient phenomena in porous media with special regard to concrete durability, Journal of Advanced Cement Based Materials 6 (3–4) (1997) 71–75.
[22] JSCE, JSCE Standard Specification for Concrete Structures (Construction), Society of Civil Engineering, Tokyo, Japan, 2002.
[23] J.S. Kong, A.N. Ababneh, D.M. Frangopol, Y. Xi, Reliability analysis of chloride penetration in saturated concrete, Journal of Probabilistic Engineering Mechanics 17 (3) (2002) 302–315.
[24] T. Luping, L.-O. Nilsson, Chloride binding capacity and binding isotherms of OPC pastes and mortars, Journal of Cement and Concrete Research 23 (2) (1993) 247–253.
[25] B. Martin-Perez, S.J. Pantzopoulou, M.D.A. Thomas, Numerical solution of mass transport equations in concrete structures, Journal of Computers and Structures 79 (13) (2001) 1251–1264.

[26] R. Mc Gee, Modeling of durability performance of Tasmanian bridges, Proceedings of the ICASP8 Conference, 297–306, Sydney, Australia, 1999.
[27] A. Neville, Properties of Concrete, 4th Edition John Wiley & Sons, Inc., 1996.
[28] National oceanic and atmospheric administration (NOAA), www.noaa.gov.
[29] C.L. Page, N.R. Short, A. El Tarras, Diffusion of chloride ions in hardened cement paste, Journal of Cement and Concrete Research 11 (3) (1981) 395–406.
[30] V.G. Papadakis, C.G. Vayenas, M.N. Fardis, Fundamental modeling and experimental investigation of concrete carbonation, ACI Materials Journal (1991) 363–373 Title No. 88-M43.
[31] Powers, T.C. and Brownyard, T.L. (1946–1947). Proceedings of American Concrete Institute, 43, 101, 149, 469, 549, 845, 933.
[32] Radjy, F. (1968). A thermodynamic study of the system hardened cement paste and water and its dynamic mechanical response as a function of temperature. Ph.D. Dissertation, Stanford University.
[33] A. Saetta, R. Scotta, R. Vitdiani, Analysis of chloride diffusion into partially saturated concrete, ACI Materials Journal 90 (5) (1993) 441–451.
[34] A. Saetta, B.A. Scherefler, R.V. Vitaliani, 2-D model for carbonation and moisture/heat flow in porous materials, Journal of Cement and Concrete Research 25 (8) (1995) 1703–1712.
[35] A. Saetta, R.V. Vitaliani, Experimental investigation and numerical modeling of carbonation process in reinforced concrete structures, Part I. Theoretical formulation, Journal of Cement and Concrete Research 34 (4) (2004) 571–579.
[36] A. Saetta, R. Vitdiani, Experimental investigation and numerical modeling of carbonation process in reinforced concrete structures, Part II. Practical applications, Journal of Cement and Concrete Research 35 (5) (2005) 958–967.
[37] Shafei, B. (2011). Stochastic finite-element analysis of reinforced concrete structures subjected to multiple environmental stressors. Ph.D. Dissertation, University of California, Irvine.
[38] K.A. Snyder, Validation and modification of the 4SIGHT computer program, , 2001 NISTIR 6747.
[39] A. Steffens, D. Dinkler, H. Ahrens, Modeling carbonation for corrosion risk prediction of concrete structures, Journal of Cement and Concrete Research 32 (6) (2002) 925–941.
[40] M. Stewart, D. Rosowsky, Time-dependent reliability of deteriorating reinforced concrete bridge decks, Journal of Structural Safety 20 (1) (1998) 91–109.
[41] D.V. Val, Aspects of corrosion in reinforced concrete structures and its influence on structural safety. Report No. 2002950, National Building Research Institute, 2004.
[42] J.C. Walton, L.E. Plansky, R.W. Smith, Models for estimation of service life of concrete barriers in low-level radioactive waste disposal, Report prepared for U.S. Nuclear Regulatory Commission, NUREG/CR-5542 EGG-2597, 1990.
[43] Y. Xi, Z.P. Bazant, H.M. Jennings, Moisture diffusion in cementitious materials: adsorption isotherms, Journal of Advanced Cement Based Material 1 (6) (1994) 248–257.
[44] Y. Xi, Z.P. Bazant, H.M. Jennings, Moisture diffusion in cementitious materials: moisture capacity and diffusivity, Journal of Advanced Cement Based Material 1 (6) (1994) 258–266.
[45] Y. Xi, Z.P. Bazant, Modeling chloride penetration in saturated concrete, Journal of Materials in Civil Engineering 11 (1) (1999) 58–65.